Accepted Manuscript

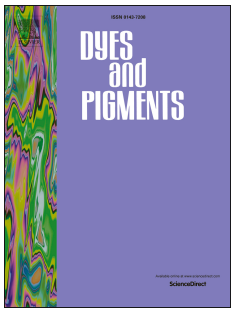

Triphenylamine-modified difluoroboron dibenzoylmethane derivatives: Synthesis, photophysical and electrochemical properties

Hao Zhang, Chun Liu, Jinghai Xiu, Jieshan Qiu

PII: S0143-7208(16)30733-1

DOI: 10.1016/j.dyepig.2016.09.036

Reference: DYPI 5488

To appear in: *Dyes and Pigments*

Received Date: 21 July 2016

Revised Date: 12 September 2016

Accepted Date: 13 September 2016

Please cite this article as: Zhang H, Liu C, Xiu J, Qiu J, Triphenylamine-modified difluoroboron dibenzoylmethane derivatives: Synthesis, photophysical and electrochemical properties, *Dyes and Pigments* (2016), doi: 10.1016/j.dyepig.2016.09.036.

Graphical Abstract

Triphenylamine-modified difluoroboron dibenzoylmethane derivatives: synthesis, photophysical and electrochemical properties

Hao Zhang, Chun Liu,* Jinghai Xiu and Jieshan Qiu

[*] Dr. C. Liu, Corresponding Author
State Key Laboratory of Fine Chemicals, Dalian University of Technology, Linggong Road 2, Dalian 116024, China.
Tel.: +86-411-84986182.
E-mail: cliu@dlut.edu.cn

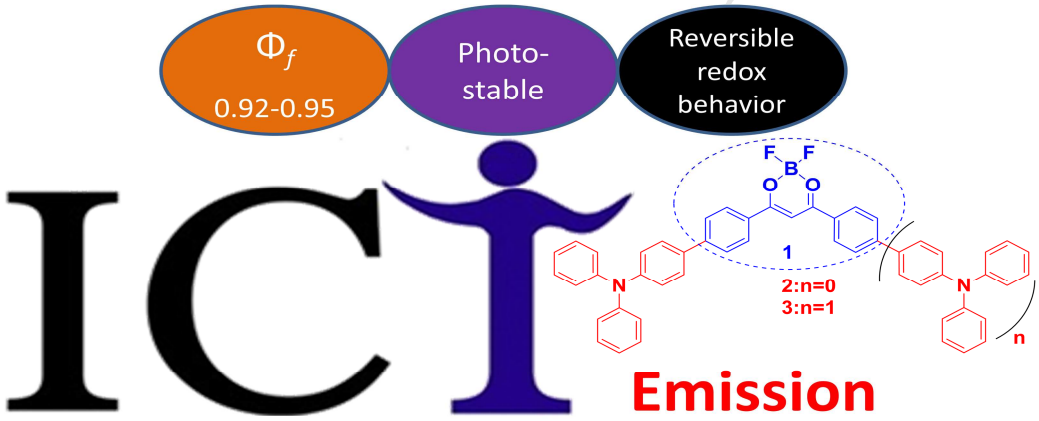

Triphenylamine-modified difluoroboron dibenzoylmethane derivatives: synthesis, photophysical and electrochemical properties

Hao Zhang, Chun Liu,* Jinghai Xiu and Jieshan Qiu

[*] Dr. C. Liu, Corresponding-Author

State Key Laboratory of Fine Chemicals, Dalian University of Technology, Linggong Road 2, Dalian 116024, China

Tel.: +86-411-84986182.

E-mail: cliu@dlut.edu.cn

Keywords: *Difluoroboron complex, Triphenylamine, ICT emission, Photostability, Polarity probe.*

Abstract:

Two new triphenylamine functionalized difluoroboron (BF_2) β-diketonate complexes, one asymmetrical **2** and the other symmetrical **3**, were synthesized and fully characterized. The effects of the triphenylamine substituent on the photoluminescence, redox properties and photostability of these BF_2 complexes were investigated. These new compounds exhibit long-wavelength absorption and strong intramolecular charge transfer emission and reversible oxidation and reduction waves in cyclic voltammetry experiments. It was found that they were highly fluorescent in toluene with large Stokes shifts, and demonstrated excellent photostability comparable to their parent BF_2 nucleus. Meanwhile, these new complexes are highly sensitive to the solvent polarity, which indicates that they could be used as highly sensitive polar probes besides excellent emitting materials.

1. Introduction

Difluoroboron complexes, classified as *N*,*N*-bidentate, *O*,*O*-bidentate and *N*,*O*-bidentate compounds [1, 2], have been extensively investigated in recent years for their various applications in bioprobes, fluorescent indicators and photosensitizers [3-9]. Among them, of particular importance are difluoroboron β-diketonate complexes, which have outstanding properties such as large molar extinction coefficients, intense emission, redox activities, high photostability and sensitivity to the surrounding medium [10-13]. Owing to these properties, they have been widely employed in near-IR probes [14, 15]. optical materials [16, 17], solar cells [18], mechanochromic luminescent materials [19, 20] and organic field-effect transistors [21]. For example, a class of difloroboron β-diketonate complexes reported by Fraser's group showed mechanochromic luminescence [22-25]. In 2015, Lu et al. prepared some luminescent organogels based on the difluoroboron complexes [26]. Untill now, many new difluoroboron complexes have been synthesized and the study on their structure-property relationship has become a research hotspot [20, 27-29].

Difluoroboron dibenzoylmethane derivatives (BF_2dbms), as a special type of difloroboron β-diketonate complexes, have also attracted considerable attention as fluorophores due to their unique optical properties [17, 30, 31]. Recently, Wang et al. reported the synthesis and spectrocopic properties of new diaroylmethanatoboron difluoride derivatives [32]. In 2013, Gao et al.

investigated the aggregation-induced emission of difluroboron dibenzoylmethane derivatives [31].

Triphenylamine (TPA) has been used as a building block to construct numerous organic electro-luminescent materials [33-36], because of its noncoplanarity of the three phenyl substituents, strong electron donor, prominent light-to-electrical energy conversion efficiencies, and good hole transporting capability. A series of new bis- and tris-β-diketone-boron difluorides using TPA as the terminal groups have been also reported by Lu et al [36-38]. More recently, Ono and coworkers have synthesized difluoroboron complexes containing *n*-butyl-substituted TPA moiety and investigated their photoluminescence properties. These complexes could be used to fabricate dye-sensitized solar cells, providing the conversion efficiencies in a range of 2.7-4.4% [35]. However, TPA-modified asymmetrical and symmetrical difluoroboron complexes based on BF_2dbm (**1**, Scheme 1) have not been reported. In this work, we design and synthesize two new TPA-bearing difluoroboron complexes **2** (asymmetrical, Scheme 1) and **3** (symmetrical, Scheme 1) to understand how the TPA moiety affect the properties of the corresponding complexes and what the differences in photoelectric performances between symmetrical and asymmetric TPA-modified difluoroboron complexes are.

In this paper, an asymmetric compound **2** and a symmetric complex **3** have been successfully synthesized (Scheme 1). Investigations on the

structure-property relationships, such as photostability, optical and electrochemical properties, have been carried out. Meanwhile, theoretical calculations (DFT) were also performed to support and provide further insights into our experimental findings. Interestingly, the results show that **3** is able to monitor the ethanol contents in toluene with a limit of detection up to 0.0091%.

Here Scheme 1. Molecular structures of complexes **1**, **2** and **3**.

2. Experimental

2.1 Materials and measurements

CH_2Cl_2 was freshly distilled from CaH_2. All the other chemicals and reagents were purchased from commercial sources and used without further purification. ^{1}H NMR, ^{13}C NMR and ^{19}F NMR spectra were recorded on a 400 MHz Varian Unity Inova spectrophotometer. Mass spectra were recorded with a MALDI micro MX spectrometer. UV-vis absorption spectra were recorded by Lambda 750S UV/vis/NIR spectrophotometer (PerkinElmer). Fluorescence emission spectra were recorded by HITACHI F-7000 fluorescence spectrophotometer. Fluorescence lifetimes were determined on a steady and transient state fluorometer (FLS920, Edinburgh Analytical Instruments Ltd.). IR spectra were recorded on a FTIR NEXUS Spectrometer using KBr disks and wave numbers were given in cm^{-1}. Melting points were determined using X-4 digital melting point apparatus. Cyclic voltammograms of all the difluoroboron β-diketonate complexes were recorded on an electrochemical

workstation (BAS100B/W, USA) at room temperature. Crystallographic data were collected using a Bruker SMART CCD diffractometer and graphite−monochromated Mo−K_α radiation (λ = 0.71073 Å).

2.2 Synthesis

Compound **8** [39] and ligands **5**-**6** [40] were conveniently synthesized according to the literature method and then used to synthesize difluoroboron β-diketonate complexes via a distinctive step as previously reported (Scheme 2) [41].

*2.2.1. Compound **8**.*

Sodium hydride (0.19 g, 8.0 mmol) was added quickly to a dry flask containing a solution of methyl benzoate (1.25 mL, 10.0 mmol) in 20 mL of dry THF. The mixture was heated to 60 °C. 1-(4-Bromophenyl)ethanone (0.99 g, 5.0 mmol) in dry THF (20 mL) was added dropwise to the mixture. The reaction mixture was refluxed under an atmosphere of nitrogen for 24 h. Then the mixture was poured into water and neutralized with hydrochloric acid until pH = 7. The mixture was extracted twice with ethyl acetate. After the solvent was removed, the residue was purified by column chromatography (silica gel, ethyl acetate/petroleumether, V/V = 300/1) to afford a pale yellow solid (1.02 g, 3.37 mmol, 66%). ^{1}H NMR (400 MHz, $CDCl_3$, 25 °C) δ 7.98 (d, *J* = 7.4 Hz, 2H, *ortho*-C_6H_5), 7.86 (d, *J* = 8.6 Hz, 2H, *ortho*-C_6H_4), 7.63 (d, *J* = 8.6 Hz, 2H, *meta*-C_6H_4), 7.57 (t, *J* = 7.4Hz, 1H, *para*-C_6H_5), 7.50 (t, *J* = 7.4 Hz, 2H, *meta*-C_6H_5), 6.82 (s, 1H, CHCO) (Fig. S3).

*2.2.2. Ligand **5**.*

A mixture of 4-(diphenylamino)phenylboronic acid (0.29 g, 2.0 mmol), compound **8** (0.30 g, 1.0 mmol), and K_2CO_3 (0.21 g, 1.5 mmol) in distilled water (9 mL) and THF (15 mL) was charged and bubbled by nitrogen for 20 min, and then $Pd(PPh_3)_4$ (20.0 mg, 0.017 mmol) was added. The mixture was refluxed for 24 h under nitrogen. After cooling to room temperature, the mixture was extracted with ethyl acetate three times. Then the organic phase was combined and dried over anhydrous Na_2SO_4. After removing the solvent under reduced pressure, the residue was purified by column chromatography (silica gel, petroleum ether/ethyl acetate, V/V = 100/1) to give a light yellow solid (0.28 g, 0.60 mmol, 60%). ^{1}H NMR (400 MHz, $CDCl_3$, 25 °C) ^{1}H NMR (400 MHz, $CDCl_3$, 25 °C) δ 8.05 – 7.86 (m, 4H, *ortho*-C_6H_5CO, C_6H_4CO), 7.62 (d, J = 8.6 Hz, 2H, *meta*-C_6H_4CO), 7.55 – 7.37 (m, 5H, *meta*-, *para*-C_6H_5CO, C_6H_4), 7.31 – 7.19 (m, 4H, *meta*-C_6H_5), 7.14 – 7.00 (m, 8H, *ortho*-, *para*-C_6H_5, C_6H_4), 6.90 (s, 1H, CHCO) (Fig. S4).

*2.2.3. Compound **10.***

A mixture of 4-(diphenylamino)phenylboronic acid (0.29 g, 2.0 mmol), compound **7** (0.19 g, 1.0 mmol), and K_2CO_3 (0.21 g, 1.5 mmol) in distilled water (4 mL) and ethanol (12 mL) was charged and then $Pd(OAc)_2$ (23.0 mg, 0.10 mmol) was added. The mixture was refluxed for 3 h, monitored by TLC (petroleum ether/ethyl acetate, V/V = 10/1). After cooling to room temperature, the saturated salt water was added and the mixture was extracted with ethyl acetate for three times. Then the organic phase was combined and dried over anhydrous Na_2SO_4. After removing the solvent under reduced pressure, the residue was purified by column chromatography (silica

gel, petroleum ether/ethyl acetate, V/V = 50/1) to give a yellow green solid (0.39 g, 1.07 mmol, 98%). ^{1}H NMR (400 MHz, $CDCl_3$, 25 °C) δ 8.01 (d, *J* = 8.4 Hz, 2H, C_8H_7O), 7.66 (d, *J* = 8.4 Hz, 2H, C_8H_7O), 7.51 (d, *J* = 8.8 Hz, 2H, C_6H_4), 7.31 – 7.26 (m, 4H, *meta*-C_6H_5), 7.16 – 7.01 (m, 8H, *ortho*-, *para*-C_6H_5, C_6H_4), 2.63 (s, 3H, CH_3) (Fig. S5).

*2.2.4. Compound **11**.*

A mixture of 4-(diphenylamino)phenylboronic acid (0.29 g, 2.0 mmol), compound **9** (0.21 g, 1.0 mmol), and K_2CO_3 (0.21 g, 1.5 mmol) in distilled water (4 mL) and ethanol (12 mL) was charged and then $Pd(OAc)_2$ (23.0 mg, 0.10 mmol) was added. The mixture was refluxed for 3 h, monitored by TLC (petroleum ether:ethyl acetate, V/V = 10:1). After cooling to room temperature, the saturated salt water was added and the mixture was extracted with ethyl acetate for three times. Then the organic phase was combined and dried over anhydrous Na_2SO_4. After removing the solvent under reduced press, the residue was purified by column chromatography (silica gel, petroleum ether/ethyl acetate, V/V = 50/1) to give a yellow green solid (0.36 g, 0.95 mmol, 96%). ^{1}H NMR (400 MHz, $CDCl_3$, 25 °C) *δ* 8.08 (d, *J* = 8.4 Hz, 2H, $C_8H_7O_2$), 7.63 (d, *J* = 8.4 Hz, 2H, $C_8H_7O_2$), 7.50 (d, *J* = 8.7 Hz, 2H, C_6H_4), 7.29 – 7.26 (m, 4H, *meta*-C_6H_5), 7.18 – 7.01 (m, 8H, *ortho*-, *para*-C_6H_5, C_6H_4), 3.93 (s, 3H, OCH_3) (Fig. S6).

*2.2.5. Ligand **6**.*

Sodium hydride (0.048 g, 2.0 mmol) was added quickly to a dry flask containing a solution of compound **11** (0.19 g, 0.5 mmol) in 10 mL of dry THF. The mixture was heated to 60 ^{o}C. Compound **10** (0.18 g, 0.5 mmol) in dry THF (10 mL) was added dropwise to the mixture. The reaction mixture was refluxed under an atmosphere of nitrogen for 24 h. Then the mixture was poured into water and neutralized with hydrochloric acid until pH = 7. And the mixture was extracted twice with ethyl acetate. After the solvent was removed, the residue was purified by column chromatography (silica gel, ethyl acetate/petroleum ether, V/V = 100/1) to afford a pale yellow solid (0.17 g, 0.24 mmol, 46%). Mp: 113 – 115 °C. ^{1}H NMR (400 MHz, $CDCl_3$, 25 °C) δ 8.07 (d, J = 8.4 Hz, 4H, C_6H_4CO), 7.71 (d, J = 8.4 Hz, 4H, C_6H_4CO), 7.55 (d, J = 8.7 Hz, 4H, C_6H_4), 7.33 – 7.27 (m, 8H, *meta*-C_6H_5), 7.17 - 7.02 (m, 16H, *ortho*-, *para*-C_6H_5, C_6H_4), 6.93 (s, 1H, CHCO) (Fig. S7). ^{13}C NMR (100MHz, $CDCl_3$, 25 °C) δ = 184.8, 183.7, 147.8, 147.1, 144.3, 133.4, 132.9, 129.0, 127.7, 127.4, 126.3, 124.4, 123.0, 92.6 (Fig. S8). IR (KBr): ν = 3433, 2960, 2921, 1734, 1589, 1488, 1379, 1327, 1278, 1197, 825, 788, 753, 696, 617, 511 cm^{-1}. MALDI-TOF-MS (m/z): calcd for $C_{51}H_{38}N_2O_2$ $[M]^+$ 710.2933; found 710.2956 (Fig. S9).

*2.2.6. Complex **1**.*

Boron trifluoride–diethyl etherate (0.13 mL, 1.0 mmol) was added to a solution of compound **4** (0.11 g, 0.5 mmol) in dry dichloromethane (15 mL) under nitrogen. The reaction mixture was stirred for 2 h. After removal of the solvent, the residue was purified by chromatography on silica gel (petroleum ether/dichloromethane, V/V = 5/1) to afford a light yellow solid (0.088 g, 0.32 mmol, 65%). ^{1}H NMR (400 MHz,

$CDCl_3$, 25 °C) δ 8.13 (d, J = 7.5 Hz, 4H, *ortho*-C_6H_5) 7.68 (t, J = 7.5 Hz, 2H, *para*-C_6H_5), 7.54 (t, J = 7.5 Hz, 4H, *meta*-C_6H_5), 7.20 (s, 1H, CHCO) (Fig. S10).

2.2.7. Complex ***2.***

Boron trifluoride–diethyl etherate (0.13 mL, 1.0 mmol) was added to a solution of compound **5** (0.095 g, 0.2 mmol) in dry dichloromethane (15 mL) under nitrogen. The reaction mixture was stirred for 2 h. After removal of the solvent, the residue was purified by chromatography on silica gel (petroleum ether/dichloromethane, V/V = 1/1) to afford a bright red solid (0.061 g, 0.12 mmol, 60%). Mp: 254 – 256 °C. ^{1}H NMR (400 MHz, $CDCl_3$, 25 °C) δ 8.21-8.17 (m, 4H, *ortho*-C_6H_5CO, C_6H_4CO), 7.76 (d, J = 8.4 Hz, 2H, *meta*-C_6H_4CO), 7.63 – 7.48 (m, 5H, *meta*-, *para*-C_6H_5CO, C_6H_4), 7.35 – 7.27 (m, 4H, *meta*- C_6H_5), 7.22 (s, 1H, CHCO), 7.19 – 7.05 (m, 8H, *ortho*-, *para*-C_6H_5, C_6H_4) (Fig. S11). ^{13}C NMR (100 MHz, $CDCl_3$, 25 ^{o}C) δ= 182.7, 148.9, 147.6, 147.2, 135.0, 130.9, 129.7, 129.5, 129.3, 128.9, 128.1, 126.8, 125.1, 123.7, 122.8, 93.2 (Fig. S12). ^{19}F NMR (376 MHz, $CDCl_3$, 25 ^{o}C) δ = -139.95, -140.01 (Fig. S13). IR (KBr): ν = 3063, 2960, 1727, 1589, 1549, 1487, 1373, 1280, 1162, 1043, 828, 807, 772, 755, 697, 613, 511 cm^{-1}. MALDI-TOF-MS (m/z): calcd for $C_{33}H_{24}NO_2F_2B$ $[M]^+$ 515.1868; found 515.1843 (Fig. S14).

2.2.8. Complex ***3****.*

Boron trifluoride-diethyl etherate (0.13 mL, 1.0 mmol) was added to a solution of compound **6** (0.14 g, 0.2 mmol) in dry dichloromethane (15 mL) under nitrogen. The reaction mixture was stirred for 2 h. After removal of the solvent, the residue was purified by chromatography on silica gel (petroleum ether/dichloromethane, V/V = 1/1) to afford a dark red solid (0.045 g, 0.06 mmol, 30%). Mp: 269 – 271 °C. ^{1}H NMR (400 MHz, $CDCl_3$, 25 °C) δ 8.21 (d, J = 8.6 Hz, 4H, C_6H_4CO), 7.76 (d, J = 8.6 Hz, 4H, C_6H_4CO), 7.56 (d, J = 8.7 Hz, 4H, C_6H_4), 7.32 – 7.27 (m, 8H, *meta*-C_6H_5), 7.23 (s, 1H, CHCO), 7.17- 7.05 (m, 16H, *ortho*-, *para*-C_6H_5, C_6H_4) (Fig. S15). ^{13}C NMR (100 MHz, $CDCl_3$, 25 °C) δ = 181.5, 148.5, 147.0, 146.9, 135.1, 131.7, 130.9, 130.5, 130.1, 129.7, 129.2, 129.1, 127.7, 126.5, 124.7, 123.3, 122.5, 92.7 (Fig. S16). ^{19}F NMR (376 MHz, $CDCl_3$, 25 °C) δ = -140.05, -140.12 (Fig. S17). IR (KBr): ν = 3036, 2925, 1721, 1588, 1541, 1487, 1372, 1331, 1287, 1203, 1043, 827, 801, 756, 697, 614, 516 cm^{-1}. MALDI-TOF-MS (m/z): calcd for $C_{51}H_{37}N_2O_2BF_2$ $[M]^+$ 758.2916; found 758.2902 (Fig. S18).

4.3. X-ray structural analysis

Crystals suitable for X-ray analysis were grown by slow diffusion of n-hexane into the respective solution of **2** or **3** in chloroform at room temperature. Reflection data were collected at 296 (2) K using a graphite monochromator with Mo-K_α radiation (λ = 0.71073 Å) on a Bruker SMART APEX(II) CCD diffractometer. The collected frames were processed with the software SAINT and an absorption correction (SADABS) was used to the collected reflections. The resulting structure was solved by

the Direct or Patterson methods (SHELXTL 97) in conjunction with standard difference Fourier techniques and then refined by full-matrix least-square technique on F^2. All hydrogen atoms were positioned geometrically and non-hydrogen atoms were refined anisotropically. Relevant crystal data for the structures are collected in the Supporting Information.

3. Results and Discussion

3.1 Synthesis and characterization

The synthetic routes to the BF_2 complexes **1**, **2** and **3** were illustrated in Scheme 2. First, the Claisen condensation reaction of compound **7** with methylbenzoate in the presence of sodium hydride in anhydrous THF afforded compound **5** in a yield of 66%. Then, the Suzuki-Miyaura coupling reaction between compound **8** and 4-(diphenylamino)phenylboronic acid gave ligand **5** in a yield of 63%. Next, ligand **5** reacted with boron trifluoride-diethyl etherate directly in anhydrous CH_2Cl_2, affording **2** in a yield of 60%. Similarly, compounds **10** and **11** were synthesized from compound **7** and **9** through the Suzuki-Miyaura coupling reaction, respectively. Ligand **6** was prepared via the Claisen condensation reaction between compounds **10** and **11** in a yield of 46%. Finally, **6** reacted with boron trifluoride-diethyl etherate directly to give **3** in a yield of 30%. Complex **1**, the dibenzoylmethane skeleton was used as a reference, which was characterized by ^{1}H NMR spectroscopy. Complexes **2** and **3** were characterized by ^{1}H NMR, ^{13}C NMR, ^{19}F NMR and MALDI-TOF mass spectrometry.

Here Scheme 2. Synthetic routes to complexes **1**, **2** and **3**.

3.2 X-ray crystallographic analysis of BF_2 complexes

The molecular and crystal structures of **2** and **3** were investigated by X-ray crystallographic analysis. Single crystals of **2** and **3** suitable for X-ray diffraction analysis were obtained by slow diffusion of hexane into a solution of **2** or **3** in chloroform. ORTEP drawings of **2** and **3** are shown in Fig. 1 and selected crystallographic data are provided in Table S1 (see Supporting Information). Key bonding parameters are given in Table 1. Overall, both compounds **2** and **3** have slightly distorted tetrahedral structures with geometrical parameters in line with expectations. In the two molecules, it was found that two fluorine atoms were distributed over the different side of the diketonate six-member ring. The sp^3 orbits hydridized at boron centers of **2** appeared as a distorted tetrahedron with bond angle O1-B-O2 of 111.6° (3), slightly bigger than what is observed in **3** (109.4° (3)) owing to its asymmetric structure. And the angles of F1-B-F2 in **2** and **3** were 111.7° (4) and 111.6° (3), respectively. These bond angles are in accordance with the common difluroboron diketonate analogues [10]. In unsymmetric **2**, the B-O bonds in the BF_2-chelating moiety are not equal and these bond lengths are 1.465(5) Å and 1.496(5) Å. In the symmetric **3**, the B-O bonds are almost equivalent and these bond lengths are 1.483(5) Å and 1.488(5) Å. The average B-O bond lengths of **2** and **3** were 1.480 and 1.484 Å [35] and their average B-F bond lengths were 1.373 (5) and 1.371 (5) Å. Thus it seems that all bond lengths around the boron atom are typical for

β-diketonatate of BF_2 [42]. After the generation of the chelating BF_2 ring and introduction of the triphenylamine unit, the structural rigidity is improved and the conjugated region becomes extensive. These facts discussed above can make a contribution to the intense orange fluorescence of the novel BF_2 complexes (Table 2).

Here Fig. 1. ORTEP drawing of **2** (a) and **3** (b) (30% probability ellipsoids, hydrogen atom labels have been omitted for clarity).

Here Table 1. X-ray selected bond lengths (Å) and angles (°) around the boron atom in the BF_2 complexes.

3.3 UV-vis absorption spectra of BF_2 complexes

The UV-vis absorption and the fluorescence emission spectra of **1**, **2** and **3** in toluene are shown in Fig. 2, and the corresponding photophysical data are summarized in Table 2. As a whole, the electron-donating moiety (TPA) at the *p*-position of the phenyl ring induced a remarkable red shift of the absorption maximum. As shown in Fig. 2, **1** exhibited absorption at 300-400 nm with a large extinction coefficient, which is typical for difloroboron β-diketonate conpounds. In sharp contrast, complexes **2** and **3** displayed a broad and bathochromic absorption with λ_{max} at 462 and 493 nm, respectively. Owing to the electron donating ability of triphenylamine and the electron accepting ability of difluoroboron β-diketone moiety, that is, the strong push-pull system [43], the maximum absorption band of **2** and **3** can be ascribed to the ICT

transition, which could be supported by the solvent polarity-dependent fluorescence emission spectral changes (Fig. 7-8, Fig. S1–S2) and theoretical calculations (Fig. 5). Meanwhile, the molar absorption coefficient of the maximum absorption peak for **3** was up to 4.1×10^4 $M^{-1}cm^{-1}$, which was higher than **1** (2.9×10^4 $M^{-1}cm^{-1}$) and **2** (2.4×10^4 $M^{-1}cm^{-1}$), showing strong light harvesting abilities.

Here Fig. 2. Normalized UV-vis absorption (left) and fluorescence emission (right) spectra of BF_2 complexes; c=1.0×10^{-5} mol·dm^{-3} in toluene, 25 °C.

Here Table 2. Photophysical data of BF_2 complexes in toluene.

3.4 Fluorescent emission spectra of BF_2 complexes

The triphenylamine substituent on the BF_2dbm core **1** had significant influence on emission properties of the complexes (Fig. 2 and Table 2). When a triphenylamine moiety was introduced into the *para* position of one phenyl ring, the BF_2dbm derivative **2** exhibited the emission at 587 nm with a large red shift of 145 nm compared with **1** (442 nm). The BF_2dbm derivative **3**, a symmetric molecule, had a similar emission behavior and the emission maximum was red-shifted to 590 nm. Both **2** and **3** showed orange emission in toluene with a fluorescence quantum yield (Φ_f) of 0.92 and 0.95, respectively, while the BF_2dbm core **1** showed a blue fluorescence with a quantum yield of 0.66. According to the fluorescence properties of **2** and **3**, such as longer wavelength emissions, larger Stokes shifts, broader

emission bands and solvent polarity-dependent emission (Fig. 7-8, Fig. S1–S2), it is clear that ICT is the major mechanism responsible for these phenomenon [44]. The fluorescence lifetimes of the BF_2 complexes were also measured and the results were collected in Table 2. Complexes **1-3** exhibited a similar single-exponential decay in toluene. It was found that the introduction of a triphenylamine moiety did not make an obvious difference in terms of the fluorescence lifetime (**1**, τ_f = 3.92 ns; **2**, τ_f = 3.89 ns). However, the fluorescence lifetime shortened in ca. 25%, when two triphenylamine moieties were introduced into the complex (**3**, τ_f = 2.95 ns). Thus, the introduction of the triphenylamine moiety can significantly affect the photoluminescence properties of difluoroboron derivatives.

The fluorescence behaviors in the solid state of complexes **1-3** were further investigated. Similar to their solution behaviors, the emission was red-shifted when the electron-donating triphenylamine moiety was present (**2** and **3**) compared to the unsubstituted complex (**1**). Meanwhile, the emission band of **2** red-shifted to 686 nm in the solid state from 587 nm in toluene ($\Delta\lambda$ = 99 nm), and that of **3** red-shifted to 688 nm in the solid state from 590 nm in toluene ($\Delta\lambda$ = 98 nm). The corresponding shift was 93 nm for **1**. In the solid state, complexes **2** and **3** show strong fluorescence with sharp peaks and their solid-state emission bands are narrower than that of **1**. The reason for this might be that the introduction of triphenylamine moiety increases the steric hindrance, prevents the molecules from packing compactly and thus avoids the spectral broadening.

Here Fig. 3. Emission spectra of complexes **1-3** in the solid state (λ_{ex} = 350 nm for **1**; λ_{ex} = 400 nm for **2** and **3**).

3.5 Electrochemical properties of BF_2 complexes

The electrochemical properties of **1-3** were examined using cyclic voltammetry. The redox curves are shown in Fig. 4 and the corresponding frontier orbital energy levels based on the redox data are summarized in Table 3. Using Bu_4NPF_6 (0.1 M) as the supporting electrolyte, values were obtained at a scan rate of 100 $mV \cdot s^{-1}$ with a saturated calomel electrode (SCE) as the standard [45]. As for **1**, no oxidation waves were observed up to +2.0 V versus SCE and it gave one well-defined reversible peak with half-wave potential ($E_{red}^{1/2}$) of -0.92 V. Presumably, the oxidation for **1** occured outside the potential window, due to the electron-poor nature of the BF_2 chelate. This also indicated that the HOMO energy of **1** was lower than those of **2** and **3** because of the presence of the electron-donating triphenylamine moiety. Compared with **1**, the voltammograms of **2** and **3** displayed reversible oxidation and reduction waves (Fig. 4), indicating that compounds **2** and **3** had amphoteric redox properties. The halfwave oxidation potentials ($E_{ox}^{1/2}$) for **2** and **3** were observed at +0.96 V and +0.97 V versus the SCE, respectively. The halfwave reduction potentials ($E_{red}^{1/2}$) were -0.96 (**2**), and -0.94 (**3**), which were close to the halfwave reduction potential of **1** (-0.92 V). Compared with **1**, the $E_{red}^{1/2}$ of **2** and **3** showed a slightly negative shift due to the electron-donating effect of triphenylamine moiety. From the results in Fig. 4 and the redox potential data in Table 3, we can calculate the energy gaps of **1**, **2**, and **3** in the

order of 3.12 eV (**1**) > 2.37 eV (**2**) > 2.28 eV (**3**).

Here Fig. 4. Cyclic voltammograms of complexes **1**, **2** and **3** in CH_2Cl_2.

Here Table 3. Frontier orbital energy levels of all BF_2 complexes.

3.6 Theoretical calculations (DFT)

To gain an insight into the electronic structures and understand the nature of excited states of BF_2 complexes, DFT calculations were performed at the B3LYP/6-31G(d) level with the Gaussian 09W program package [46]. The HOMO and LUMO energy diagrams of **1**, **2** and **3** were shown in Fig. 5. It is clear that the HOMO and LUMO densities of **1** are localized over the whole molecule. However, for **2**, the HOMO and LUMO densities are mainly located on the triphenylamine moiety and the BF_2dbm unit, respectively. The HOMO and LUMO densities of **3** were also clearly separated from each other. These results also further demonstrate that the ICT process predictably occurs from the donor to the acceptor moiety in **2** and **3**. The HOMO-LUMO gaps for **1, 2** and **3** are 3.84 eV, 2.23 eV and 2.21 eV, respectively, which is nearly in agreement with the results based on the emission spectra and electrochemical data (Table 3). Both the HOMO and LUMO energy increase when triphenylamine group was introduced into the *para* position of the phenyl rings. Clearly, introducing the triphenylamine group into the BF_2dbm compounds affects the HOMO level significantly, resulting in a marked decrease in energy gap (*E*g).

Here Fig. 5. HOMO and LUMO energies (eV) of complexes **1-3** calculated by using DFT at the B3LYP/6-31G(d) level.

3.7 Photostability of BF_2 complexes

The photostability of BF_2 complexes under continuous irradiation was studied according to the method described by Hartmann and co-workers [47], to test their potential practical applications as new emitting materials. In this work, the BF_2 complex was immobilized in an ethylcellulose (EC) film and its weight content is 0.5 wt%. The thickness of the film is about 5.88 μm. Photostability of EC films immobilized with BF_2 complexes were estimated upon continuous irradiation with a 254 nm 16 W UV lamp under air atmosphere. The power density on the films is 21.5 W/m^2. The photostability of **2** and **3** were studied by continuous irradiation and were compared with that of the known **1**. Both complexes **2** and **3** showed better photostability than that of **1** (Fig. 6). In fact, 11% and 6% decreases in the fluorescence intensity of **2** and **3** were observed respectively (60 min), compared to 52% for **1**. The results demonstrate that the introduction of a triphenylamine moiety into the molecules of the BF_2dbm core could enhance the photostability of the corresponding complexes efficiently.

Here Fig. 6. Photo-degradation histogram of **1**, **2** and **3** immobilized in ethyl cellulose. Irradiation is performed with a WFH-204B 254 nm UV lamp. The power density on the films is 21.5 W/m^2.

3.8 The changes of the fluorescent intensity of BF_2 complexes in Ethanol/Toluene system

Donor-acceptor (D-A) systems [48] have drawn much attention for their optical properties and applications in chemical sensors [49], photodetectors [50], and non-linear optics [51]. Often their emission is solvent polarity sensitive, given charge separation in the excited state [52]. As shown in Fig. 7, remarkable spectral changes of **3** were observed in three common solvents with different polarity. The emission maximum had a red-shift and the fluorescence intensity declined sharply with the increase of the solvent polarity. To further study the effect of the solvent polarity on the emission, **3** was selected as a probe to test its emission in different contents of ethanol in toluene. The results in Figure 8 showed that **3** emitted intense orange fluorescence in toluene, which was quenched when a small amount of ethanol was added into the solution. In pace with the increase of ethanol fraction (vol%), the emission weakened gradually with the differing ethanol content from 0 to 30.0%. When the ethanol content was up to 20.0%, the emission peak almost vanished and the emission intensity decreased by 90.4%. Moreover, it was found that the fluorescence emission bands of **3** red-shifted significantly with the increase of the ethanol content (or the solvent polarity), accompanied by the broadening of the emission. These emission bands with the increase of the polarity of the solvents demonstrate the ICT emission feature of **3** [37, 38, 53].

Here Fig. 7. Fluorescence spectral variation of **3** (10 μmol/L) in different solvents.

Here Fig. 8. Fluorescence spectral variation of **3** (10 μmol/L) in toluene with different ethanol contents (volume fraction 0-30.0%, λ_{ex} = 400 nm).

Similarly, the fluorescence properties of **1** and **2** were then investigated in the EtOH/Toluene mixture at various ratios to compare the emission changes to the solvent polarity (Fig. 9, and Fig. S1–S2). In Fig. 9, the quenching rate is the Y-axis and the ethanol fraction (δ(EtOH)/%) is the X-axis. It was clear that the quenching rates of **1**, **2** and **3** were observed at 45.9%, 98.1% and 90.4% respectively, when the content of ethanol was 20.0%. Therefore, the sensitivity of the emission of BF_2 complexes to the solvent polarity is in the sequence of **2** > **3** > **1**. The results demonstrate that complexes **2** and **3** are potential sensor molecules for communicating local environmental properties.

Here Fig. 9. Quenching rates of fluorescence intensity of **1**, **2**, and **3** (10 μmol/L) to different ethanol contents in toluene at λ_{em} = 450 nm for **1**; λ_{em} = 600 nm for **2** and **3** (λ_{ex} = 350 nm for **1**; λ_{ex} = 400 nm for **2** and **3**).

Meanwhile, by fitting the fluorescence spectra data of **2** and **3** at λ_{em} = 600 nm in the EtOH/Toluene mixture at various ratios, we found that the fluorescence intensity of **3** showed an excellent linear relationship with the ethanol fraction when the content of ethanol was in the range of 0 to 3.0% (Figure 10). The linear equation could be

described as follows: **I** =1380.2-184.3×100**δ**(EtOH). The correlation coefficient is 0.995. Then the limit of detection (LOD) of this method was evaluated by the linear regression equation. The algorithm can be described as follows:

$$LOD = 3S/K \qquad \text{Eq. 1}$$

In this equation, S is the relative standard deviation whose numerical value is obtained after enough blank tests. K is the slope of the linear regression equation. The results of eleven blank tests showed that the relative standard deviation (S) was 0.56%. The LOD of this method was obtained according to Eq. 1. Complex **3** can be used as a polar sensitive probe to monitor the ethanol content in toluene directly, with a detection limit of 0.0091%.

Here Fig. 10. Response of fluorescence intensity at λ_{em} = 600 nm of **3** (10μmol/L) to different ethanol contents in toluene (λ_{ex} = 400 nm).

4. Conclusions

In summary, novel triphenylamine-substituted BF_2 complexes **2** and **3** have been synthesized and characterized by means of spectroscopic, electrochemical methods and X-ray crystal structure. These compounds exhibit long wavelength absorptions in their UV-vis spectra and a red shift of the emission, and demonstrate enhanced photostability compared to unmodified **1**. Both **2** and **3** emit intense orange light in toluene with the Φ_f up to 0.92 and 0.95, respectively. The electrochemical

voltammograms of these complexes illustrate reversible oxidation and reduction waves. Meanwhile, the TPA-modified complexes are highly sensitive to the solvent polarity of the mixture of ethanol/toluene.

Acknowledgment

The authors thank the financial support from the National Natural Science Foundation of China (21276043 and 21421005), and Open Fund of Key Laboratory of Biotechnology and Bioresources Utilization (Dalian Minzu University), State Ethnic Affairs Commission & Ministry of Education.

Appendix A. Supplementary data

Characterization data, NMR and MS spectra of complexes, crystal structure data, and fluorescence spectral variation curves of **1** and **2** in ethanol / toluene system. Supplementary data related to this article can be found at

Notes and references

[1] Cardona F, Rocha J, Silva AMS, Guieu S. Δ^1 -pyrroline based boranyls: Synthesis, crystal structures and luminescent properties. Dyes Pigm 2014;111:16-20.

[2] Guieu S, Cardona F, Silva AMS. Luminescent bi-metallic fluoroborate derivatives of bulky salen ligands. New J Chem 2014;38(11):5411-4.

[3] Maeda H, Kusunose Y. Dipyrrolyldiketone Difluoroboron Complexes: Novel Anion Sensors With C - H··· X− Interactions. Chem – Eur J 2005;11(19):5661-6.

[4] Loudet A, Burgess K. BODIPY dyes and their derivatives: syntheses and spectroscopic properties. Chem Rev 2007;107(11):4891-932.

[5] Itoh K, Okazaki K, Fujimoto M. The structure of 1, 3-enaminoketonatoboron difluorides in solution and in the solid state. Aust J Chem 2003;56(12):1209-14.

[6] Risko C, Zojer E, Brocorens P, Marder S, Brédas J-L. Bis-aryl substituted dioxaborines as electron-transport materials: a comparative density functional theory investigation with oxadiazoles

and siloles. Chem Phys 2005;313(1):151-7.

[7] Yogo T, Urano Y, Ishitsuka Y, Maniwa F, Nagano T. Highly efficient and photostable photosensitizer based on BODIPY chromophore. J Am Chem Soc 2005;127(35):12162-3.

[8] Oleynik P, Ishihara Y, Cosa G. Design and synthesis of a BODIPY-α-tocopherol adduct for use as an off/on fluorescent antioxidant indicator. J Am Chem Soc 2007;129(7):1842-3.

[9] Rohde D, Yan C-J, Wan L-J. C-H···F Hydrogen Bonding: The Origin of the Self-Assemblies of Bis (2, 2'-difluoro-1, 3, 2-dioxaborine). Langmuir 2006;22(10):4750-7.

[10] Ono K, Yoshikawa K, Tsuji Y, Yamaguchi H, Uozumi R, Tomura M, et al. Synthesis and photoluminescence properties of BF2 complexes with 1,3-diketone ligands. Tetrahedron 2007;63(38):9354-8.

[11] Felouat A, D'Aléo A, Fages Fr. Synthesis and Photophysical Properties of Difluoroboron Complexes of Curcuminoid Derivatives Bearing Different Terminal Aromatic Units and a meso-Aryl Ring. J Org Chem 2013;78(9):4446-55.

[12] Tanaka K, Tamashima K, Nagai A, Okawa T, Chujo Y. Facile modulation of optical properties of diketonate-containing polymers by regulating complexation ratios with boron. Macromolecules 2013;46(8):2969-75.

[13] Xu S, Evans RE, Liu T, Zhang G, Demas J, Trindle CO, et al. Aromatic difluoroboron β-diketonate complexes: effects of π-conjugation and media on optical properties. Inorg Chem 2013;52(7):3597-610.

[14] Poon C-T, Lam WH, Wong H-L, Yam VW-W. A versatile photochromic dithienylethene-containing β-diketonate ligand: near-infrared photochromic behavior and photoswitchable luminescence properties upon incorporation of a boron (III) center. J Am Chem Soc 2010;132(40):13992-3.

[15] D'Aléo A, Gachet D, Heresanu V, Giorgi M, Fages F. Efficient NIR‐Light Emission from Solid‐State Complexes of Boron Difluoride with 2′‐Hydroxychalcone Derivatives. Chem – Eur J 2012;18(40):12764-72.

[16] Halik M, Wenseleers W, Grasso C, Stellacci F, Zojer E, Barlow S, et al. Bis (dioxaborine) compounds with large two-photon cross sections, and their use in the photodeposition of silver. Chem Commun 2003(13):1490-1.

[17] Cogné‐Laage E, Allemand JF, Ruel O, Baudin JB, Croquette V, Blanchard‐Desce M, et al. Diaroyl (methanato) boron Difluoride Compounds as Medium‐Sensitive Two‐Photon Fluorescent Probes. Chem – Eur J 2004;10(6):1445-55.

[18] Chambon S, D'Aléo A, Baffert C, Wantz G, Fages F. Solution-processed bulk heterojunction solar cells based on BF 2–hydroxychalcone complexes. Chem Commun 2013;49(34):3555-7.

[19] Krishna GR, Kiran MS, Fraser CL, Ramamurty U, Reddy CM. The Relationship of Solid‐State Plasticity to Mechanochromic Luminescence in Difluoroboron Avobenzone Polymorphs. Adv Funct Mater 2013;23(11):1422-30.

[20] Liu M, Zhai L, Sun J, Xue P, Gong P, Zhang Z, et al. Multi-color solid-state luminescence of difluoroboron β-diketonate complexes bearing carbazole with mechanofluorochromism and thermofluorochromism. Dyes pigm 2016;128:271-8.

[21] Sun Y, Rohde D, Liu Y, Wan L, Wang Y, Wu W, et al. A novel air-stable n-type organic semiconductor: 4, 4′-bis [(6, 6′-diphenyl)-2, 2-difluoro-1, 3, 2-dioxaborine] and its application in organic ambipolar field-effect transistors. J Mater Chem 2006;16(46):4499-503.

[22] Zhang G, Lu J, Sabat M, Fraser CL. Polymorphism and reversible mechanochromic luminescence

for solid-state difluoroboron avobenzone. J Am Chem Soc 2010;132(7):2160-2.

[23] Nguyen ND, Zhang G, Lu J, Sherman AE, Fraser CL. Alkyl chain length effects on solid-state difluoroboron β-diketonate mechanochromic luminescence. J Mater Chem 2011;21(23):8409-15.

[24] Zhang G, Singer JP, Kooi SE, Evans RE, Thomas EL, Fraser CL. Reversible solid-state mechanochromic fluorescence from a boron lipid dye. J Mater Chem 2011;21(23):8295-9.

[25] Sun X, Zhang X, Li X, Liu S, Zhang G. A mechanistic investigation of mechanochromic luminescent organoboron materials. J Mater Chem 2012;22(33):17332-9.

[26] Qian C, Liu M, Hong G, Xue P, Gong P, Lu R. Luminescent organogels based on triphenylamine functionalized β-diketones and their difluoroboron complexes. Org Biomol Chem 2015;13(10):2986-98.

[27] Mayoral MJ, Ovejero P, Campo JA, Heras JV, Oliveira E, Pedras B, et al. Exploring photophysical properties of new boron and palladium (II) complexes with β-diketone pyridine type ligands: from liquid crystals to metal fluorescence probes. J Mater Chem 2011;21(4):1255-63.

[28] Guieu S, Pinto J, Silva VLM, Rocha J, Silva AMS. Synthesis, Post-Modification and Fluorescence Properties of Boron Diketonate Complexes. Eur J Org Chem 2015;2015(16):3423-6.

[29] Mathew AS, Derosa CA, Demas JN, Fraser CL. Difluoroboron β-diketonate materials with long-lived phosphorescence enable lifetime based oxygen imaging with a portable cost effective camera. Anal Methods 2016;8(15):3109-14.

[30] Sakai A, Tanaka M, Ohta E, Yoshimoto Y, Mizuno K, Ikeda H. White light emission from a single component system: remarkable concentration effects on the fluorescence of 1, 3-diaroylmethanatoboron difluoride. Tetrahedron Lett 2012;53(32):4138-41.

[31] Hu J, He Z, Wang Z, Li X, You J, Gao G. A simple approach to aggregation-induced emission in difluoroboron dibenzoylmethane derivatives. Tetrahedron Lett 2013;54(32):4167-70.

[32] Wang D-J, Xu B-P, Wei X-H, Zheng J. Preparation and spectroscopic properties of some new diaroylmethanatoboron difluoride derivatives. J Fluorine Chem 2012;140:49-53.

[33] Kwon J, Kim MK, Hong J-P, Lee W, Noh S, Lee C, et al. 4, 4′, 4″-Tris (4-naphthalen-1-yl-phenyl) amine as a multifunctional material for organic light-emitting diodes, organic solar cells, and organic thin-film transistors. Org Electron 2010;11(7):1288-95.

[34] Moss KC, Bourdakos KN, Bhalla V, Kamtekar KT, Bryce MR, Fox MA, et al. Tuning the intramolecular charge transfer emission from deep blue to green in ambipolar systems based on dibenzothiophene S, S-dioxide by manipulation of conjugation and strength of the electron donor units. J Org Chem 2010;75(20):6771-81.

[35] Mizuno Y, Yisilamu Y, Yamaguchi T, Tomura M, Funaki T, Sugihara H, et al. (Dibenzoylmethanato) boron Difluoride Derivatives Containing Triphenylamine Moieties: A New Type of Electron‐Donor/π‐Acceptor System for Dye‐Sensitized Solar Cells. Chem‐Eur J 2014;20(41):13286-95.

[36] Qian C, Hong G, Liu M, Xue P, Lu R. Star-shaped triphenylamine terminated difluoroboron β-diketonate complexes: synthesis, photophysical and electrochemical properties. Tetrahedron 2014;70(25):3935-42.

[37] Zhang X, Lu R, Jia J, Liu X, Xue P, Xu D, et al. Organogel based on β-diketone-boron difluoride without alkyl chain and H-bonding unit directed by optimally balanced π–π interaction. Chem Commun 2010;46(44):8419-21.

[38] Zhang X, Liu X, Lu R, Zhang H, Gong P. Fast detection of organic amine vapors based on fluorescent nanofibrils fabricated from triphenylamine functionalized β-diketone-boron difluoride. J

Mater Chem 2012;22(3):1167-72.

[39] Zawadiak J, Mrzyczek M. UV absorption and keto–enol tautomerism equilibrium of methoxy and dimethoxy 1, 3-diphenylpropane-1, 3-diones. Spectrochim Acta, Part A 2010;75(2):925-9.

[40] Rao X, Liu C, Qiu J, Jin Z. A highly efficient and aerobic protocol for the synthesis of N-heteroaryl substituted 9-arylcarbazolyl derivatives via a palladium-catalyzed ligand-free Suzuki reaction. Org Biomol Chem 2012;10(39):7875-83.

[41] Zhang G, Chen J, Payne SJ, Kooi SE, Demas J, Fraser CL. Multi-emissive difluoroboron dibenzoylmethane polylactide exhibiting intense fluorescence and oxygen-sensitive room-temperature phosphorescence. J Am Chem Soc 2007;129(29):8942-3.

[42] Galer P, Korosec RC, Vidmar M, Sket B. Crystal structures and emission properties of the BF(2) complex 1-phenyl-3-(3,5-dimethoxyphenyl)-propane-1,3-dione: multiple chromisms, aggregation- or crystallization-induced emission, and the self-assembly effect. J Am Chem Soc 2014;136(20):7383-94.

[43] Zhao GJ, Chen RK, Sun MT, Liu JY, Li GY, Gao YL, et al. Photoinduced Intramolecular Charge Transfer and S2 Fluorescence in Thiophene - π - Conjugated Donor – Acceptor Systems: Experimental and TDDFT Studies. Chem – Eur J 2008;14(23):6935-47.

[44] Wu Y-Y, Chen Y, Gou G-Z, Mu W-H, Lv X-J, Du M-L, et al. Large Stokes shift induced by intramolcular charge transfer in N, O-Chelated Naphthyridine–BF2 complexes. Org Lett 2012;14(20):5226-9.

[45] Pavlishchuk VV, Addison AW. Conversion constants for redox potentials measured versus different reference electrodes in acetonitrile solutions at 25 C. Inorg Chim Acta 2000;298(1):97-102.

[46] Frisch M, Trucks G, Schlegel H, Scuseria G, Robb M, Cheeseman J, et al. Gaussian 09, revision B. 01. Gaussian Inc, Wallingford, CT 2010.

[47] Clark HA, Barker SL, Brasuel M, Miller MT, Monson E, Parus S, et al. Subcellular optochemical nanobiosensors: probes encapsulated by biologically localised embedding (PEBBLEs). Sens Actuators, B 1998;51(1):12-6.

[48] Grabowski ZR, Rotkiewicz K, Rettig W. Structural changes accompanying intramolecular electron transfer: focus on twisted intramolecular charge-transfer states and structures. Chem Rev 2003;103(10):3899-4032.

[49] De Silva AP, Gunaratne HN, Gunnlaugsson T, Huxley AJ, McCoy CP, Rademacher JT, et al. Signaling recognition events with fluorescent sensors and switches. Chem Rev 1997;97(5):1515-66.

[50] Peumans P, Bulović V, Forrest S. Efficient, high-bandwidth organic multilayer photodetectors. Appl Phys Lett 2000;76(26):3855-7.

[51] Meyers F, Marder S, Pierce B, Bredas J. Electric field modulated nonlinear optical properties of donor-acceptor polyenes: sum-over-states investigation of the relationship between molecular polarizabilities (. alpha.,. beta., and. gamma.) and bond length alternation. J Am Chem Soc 1994;116(23):10703-14.

[52] Zhang G, Kim SH, Evans RE, Kim BH, Demas J, Fraser CL. Luminescent Donor-Acceptor β-Diketones: Modulation of Emission by Solvent Polarity and Group II Metal Binding. J Fluor 2009;19(5):881-9.

[53] BittoloáBon S. High concentration few-layer graphene sheets obtained by liquid phase exfoliation of graphite in ionic liquid. J Mater Chem 2011;21(10):3428-31.

List of Tables:

Table 1. X-ray selected bond lengths (Å) and angles (°) around the boron atom in the BF_2 complexes.

Complexes	CCDC number	B-O1	B-O2	B-F1	B-F2	O1-B-O2	F1-B-F2
2	1445632	1.465(5)	1.496(5)	1.373(5)	1.373(5)	111.6 (3)	111.7(4)
3	1445633	1.483(5)	1.488(5)	1.363(5)	1.380(5)	109.4 (3)	111.6(3)

Table 2. Photophysical data of BF_2 complexes in toluene.

Complexes	Absorption[a] λ_{abs} (nm)	Emission λ_{em} (nm)	Φ_f[b]	τ_f (ns)[c]	$\Delta\lambda_{st}$ (nm)[d]	$\Delta\nu_{st}$ (cm^{-1})[e]
1	363 (2.9), 380 (2.5)	442	0.66	3.92 (χ^2=1.101)	62	3691
2	303 (1.8), 370 (2.1), 462 (2.4)	587	0.92	3.89 (χ^2=1.003)	125	4609
3	309 (2.9), 375 (1.8), 493 (4.1)	590	0.95	2.95 (χ^2=1.001)	97	3334

[a] Measured in toluene at a concentration of 10^{-5} M and extinction coefficients ($\varepsilon_{max} \times 10^4\ M^{-1} \cdot cm^{-1}$) are shown in parentheses.

[b] Fluorescence quantum yield determined by a standard method with Rhodamine B in ethanol (Φ_f = 0.65, λ_{ex} = 365 nm; Φ_f = 0.88, λ_{ex} = 490 nm).

[c] Fluorescence lifetime measured in toluene at a sample concentration of ca. 10^{-5} M and the excitation wavelength of the laser was 405.2 nm. All fluorescence lifetimes were fitted with single-exponential decays unless indicated.

[d] $\Delta\lambda_{st} = \lambda_{em} - \lambda_{abs}$.

[e] $\Delta\nu_{st} = \nu_{abs} - \nu_{em}$.

Table 3. Frontier orbital energy levels of all BF_2 complexes.

Complexes	$E_{ox}^{1/2}$[V] [a]	$E_{red}^{1/2}$[V] [a]	HOMO [eV] experimental [b]	LUMO [eV] experimental [c]	*E*g [eV] experimental [d]
1	—	-0.92	-6.59	-3.47	3.12
2	0.96	-0.96	-5.25	-2.88	2.37
3	0.97	-0.94	-5.29	-3.01	2.28

[a] 0.1 M $[Bu_4N]PF_6$ in CH_2Cl_2, scan rate 100·mV s^{-1}, V versus SCE.

[b] $E_{LUMO} = E_{HOMO} + Eg$.

[c] E_{HOMO} (eV) = -e(4.4 + E_{ox}), E_{LUMO} (eV) = -e(4.4 + E_{red}).

[d] Estimated from the intersection of the normalized absorption and emission spectra by equation of $Eg = 1240/\lambda_{int.}$

List of Figures:

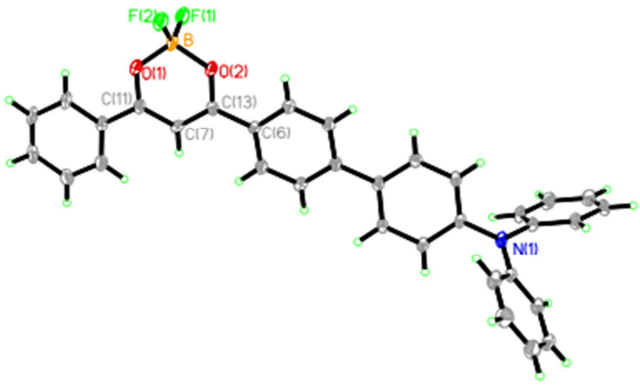

(a)

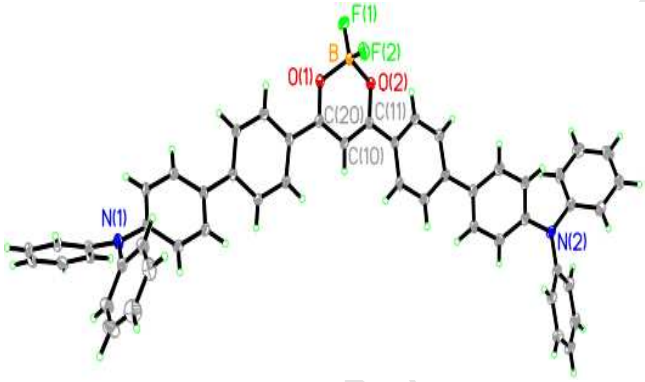

(b)

Fig. 1. ORTEP drawing of **2** (a) and **3** (b) (30% probability ellipsoids, hydrogen atom labels have been omitted for clarity).

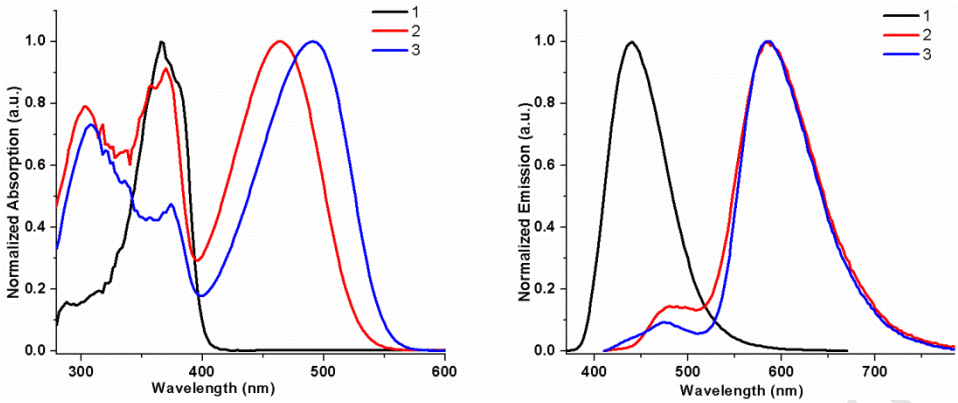

Fig. 2. Normalized UV-vis absorption (left) and fluorescence emission (right) spectra of BF_2 complexes; c = 1.0 × 10^{-5} mol·dm^{-3} in toluene, 25 °C.

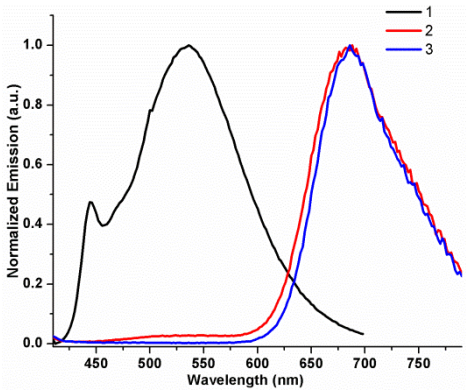

Fig. 3. Emission spectra of complexes **1-3** in the solid state (λ_{ex} = 350 nm for **1**; λ_{ex} = 400 nm for **2** and **3**).

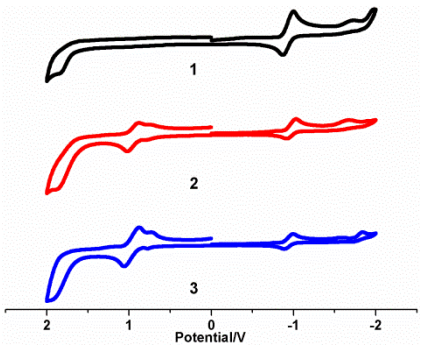

Fig. 4. Cyclic voltammograms of complexes **1**, **2** and **3** in CH_2Cl_2.

1	2	3
LUMO -3.08 eV	LUMO -3.00 eV	LUMO -2.94 eV
	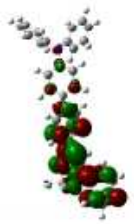	
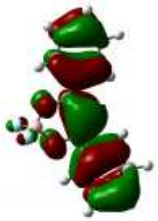	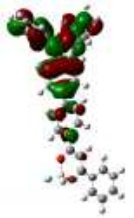	
HOMO -6.92 eV	HOMO -5.23 eV	HOMO -5.16 eV

Fig. 5. HOMO and LUMO energies (eV) of complexes **1-3** calculated by using DFT at the B3LYP/6-31G(d) level.

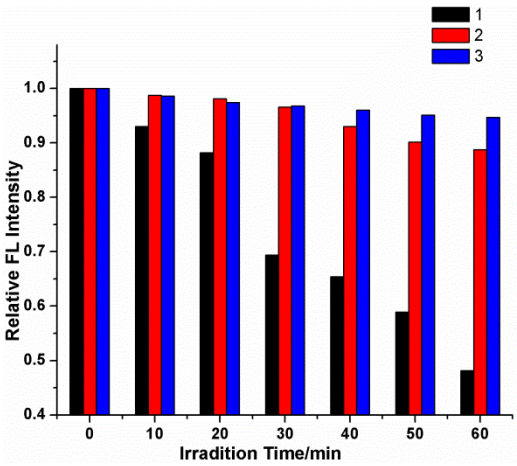

Fig. 6. Photo-degradation histogram of complexes **1**, **2** and **3** immobilized in ethyl cellulose. Irradiation is performed with a WFH-204B 254 nm UV lamp. The power density on the films is 21.5 W/m^2.

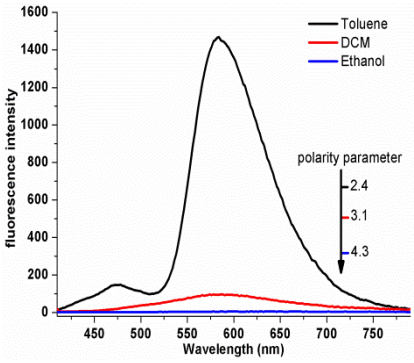

Fig. 7. Fluorescence spectral variation of **3** (10 μmol/L) in different solvents.

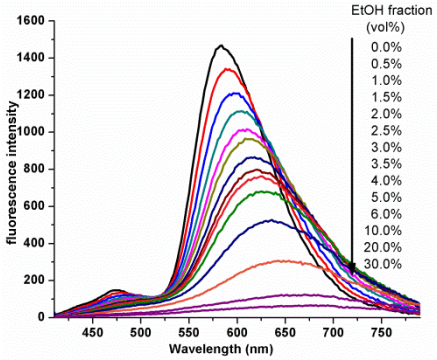

Fig. 8. Fluorescence spectral variation of **3** (10 μmol/L) in toluene with different ethanol contents (volume fraction 0-30.0%, λ_{ex} = 400 nm).

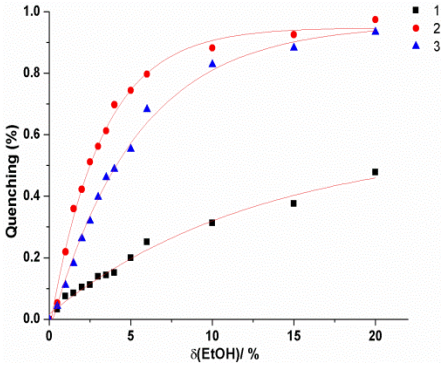

Fig. 9. Quenching rates of fluorescence intensity of **1**, **2**, and **3** (10 μmol/L) to different ethanol contents in toluene at λ_{em} = 450 nm for **1**; λ_{em} = 600 nm for **2** and **3** (λ_{ex} = 350 nm for **1**; λ_{ex} = 400 nm for **2** and **3**).

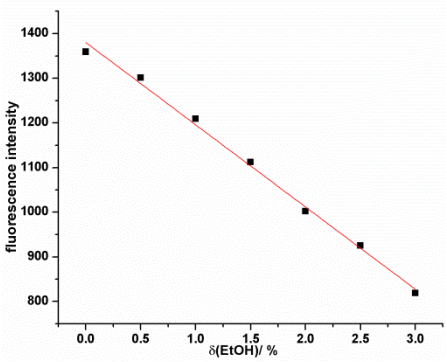

Fig. 10. Response of fluorescence intensity at λ_{em} = 600 nm of **3** (10μmol/L) to different ethanol contents in toluene (λ_{ex} = 400 nm)

List of Schemes:

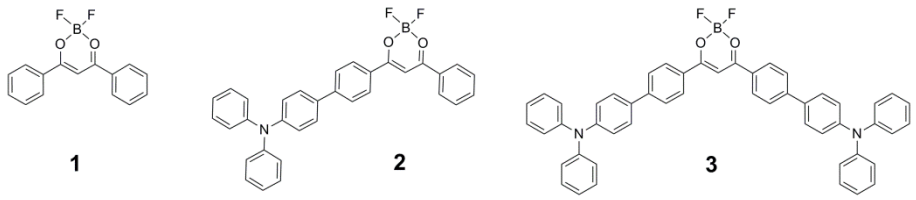

Scheme 1. Molecular structures of complexes **1**, **2** and **3**.

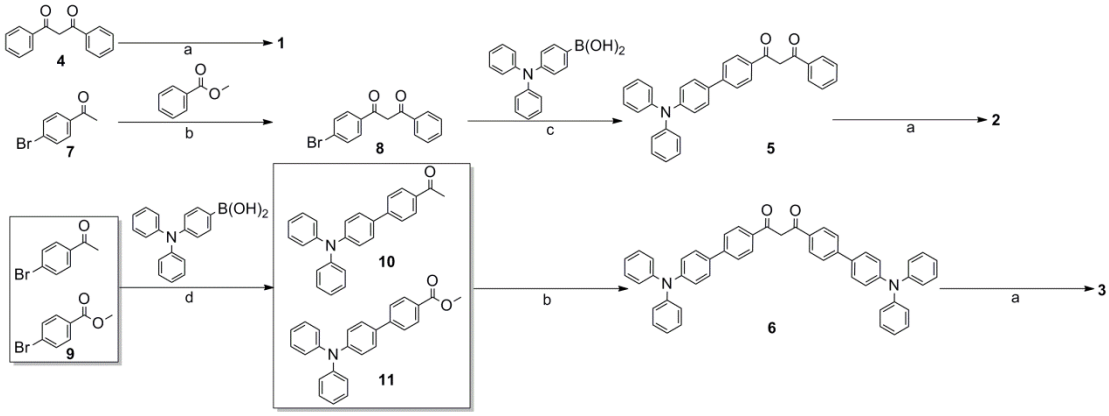

(a) $BF_3 \cdot Et_2O$, dry CH_2Cl_2; (b) NaH, THF, HCl; (c) $Pd(PPh_3)_4$, K_2CO_3, THF/H_2O; (d) $Pd(OAc)_2$, K_2CO_3, EtOH/H_2O.

Scheme 2. Synthetic routes to complexes **1**, **2** and **3**.

Research highlights

1) New TPA-modified BF_2 complexes were synthesized.
2) TPA-modified complexes demonstrate large Stokes shifts and intense ICT emissions.
3) TPA-modified complexes show enhanced photostability.
4) TPA-modified symmetric complex can detect the ethanol content in toluene.